Influence of Ligand Geometry in Bimetallic Ytterbocene Complexes of Bridging Bis(bipyridyl) Ligands

Christin N. Carlson,[†] Christopher J. Kuehl,[†] Linda Ogallo,[§] David A. Shultz,[§] J. D. Thompson,[†] Martin L. Kirk,[#] Richard L. Martin,[†] Kevin D. John,*[,†] and David E. Morris*[,†]

Los Alamos National Laboratory, Los Alamos, New Mexico 87545, Department of Chemistry, North Carolina State University, Raleigh, North Carolina 27695, and Department of Chemistry and Chemical Biology, The University of New Mexico, MSC03 2060, 1 University of New Mexico, Albuquerque, New Mexico 87131-0001

Received December 19, 2006

Two new bimetallic complexes, $[Cp^*_2Yb]_2(\mu\text{-}1,3\text{-}(2,2'\text{-bipyridyl})\text{-}5\text{-}^tBu\text{-}C_6H_3)$ (**1**) and $[Cp^*_2Yb]_2(\mu\text{-}1,4\text{-}(2,2'\text{-bipyridyl})\text{-}C_6H_4)$ (**2**), and their corresponding two-electron oxidation products $[\mathbf{1}]^{2+}$ and $[\mathbf{2}]^{2+}$ have been synthesized with the aim of determining the impact of the bridging ligand geometry on the electronic and magnetic properties of these materials. Electrochemistry, optical spectroscopy, and bulk susceptibility measurements all support a ground-state electronic configuration of the type $[(f)^{13}\text{-}(\pi_a^*)^1\text{-}(\pi_b^*)^1\text{-}(f)^{13}]$. Density functional theory calculations on the uncomplexed bridging ligands as doubly reduced species also indicate that the diradical electronic configuration is the lowest lying for both *meta*- and *para*-bis(bipyridyl) systems. The electrochemical and optical spectroscopic data indicate that the electronic coupling between the metal centers mediated by the diradical bridges is weak, as evidenced by the small separation of the metal-based redox couples and the similarity of the f−f transitions of the associated dicationic complexes ($[\mathbf{1}]^{2+}$ and $[\mathbf{2}]^{2+}$) relative to those of the monometallic $[Cp^*_2Yb(bpy)]^+$ analogue. The magnetic susceptibility data show no evidence for exchange coupling between the paramagnetic metal centers in the neutral complexes, but do indicate weak exchange coupling between Yb^{III} and ligand radical spins on each of the effectively independent halves of the bimetallic complexes. These findings are in contrast to those reported recently for $Co^{III/II}$ dioxolene bimetallic complexes bridged by these same bis(bipyridyl) ligands. The difference is attributed in part to the dominant singlet diradical character of the bridging ligands in the ytterbocene complexes. These experimental and theoretical results are consistent with expectations for organic diradical spin orientations for *meta* versus *para* substituents across a phenylene linker, but this effect does not induce significant longer-range superexchange or electronic interactions between the metal centers in these systems.

Introduction

The interesting magnetic and electronic properties found for many polypyridyl adducts of ytterbocene [$Cp^*_2Yb(L)$; $Cp^* = C_5Me_5^-$, L = 2,2′-bipyridine (bpy) (**3**), 1,10-phenanthroline (phen), 2,2′:6′,2″-terpyridine (tpy) (**7**), etc.],[1−3] in which the nominally divalent f^{14} metal center spontaneously transfers an electron into the lowest unoccupied molecular orbital (LUMO) on the polypyridyl ligand to give a stable trivalent f^{13}-ligand radical anion electronic configuration, have inspired the use of these ytterbocene polypyridyl adducts as building blocks in the design and synthesis of multimetallic f-element systems to explore the magnetic and electronic interactions between the f-element centers and the role of the bridging ligand in mediating these interactions.[4−8] In the bimetallic systems studied by Andersen and co-workers with bridging N-heterocylic ligands such as 2,2′-bipyrimidine and 2,2′-azobenzene,[4] the magnetic susceptibility data suggest that the individual ytterbocene centers behave at higher temperatures as isolated paramagnets bridged through a doubly reduced singlet ligand dianion. However, several of these systems display evidence for antiferromagnetic coupling between the ytterbocene centers at low temperature (i.e., a maximum in χ vs T is observed at ∼20 K) via a superexchange mechanism. Our studies of bimetallic ytterbocene complexes (Table 1) have, to date, focused on bridging ligands based on a tridentate polypyridyl platform ($[Cp^*_2Yb]_2(\mu\text{-L})$; L = tetra(2-pyridyl)pyrazine (tppz) (**4**), 6′,6″-bis(2-pyridyl)-2,2′;4′4″:2″,2‴-quaterpyridine (qtp) (**5**), and 1,4-di(2,2′:6′,2″-terpyridyl)benzene (*para*-diterpyridylbenzene; *p*-dtb) (**6**)) to

* Corresponding author. E-mail: kjohn@lanl.gov, demorris@lanl.gov.
[†] Los Alamos National Laboratory.
[§] North Carolina State University.
[#] The University of New Mexico.

(1) Da Re, R. E.; Kuehl, C. J.; Brown, M. G.; Rocha, R. C.; Bauer, E. D.; John, K. D.; Morris, D. E.; Shreve, A. P.; Sarrao, J. L. *Inorg. Chem.* **2003**, *42*, 5551−5559.
(2) Schultz, M.; Boncella, J. M.; Berg, D. J.; Tilley, T. D.; Andersen, R. A. *Organometallics* **2002**, *21*, 460−472.
(3) Veauthier, J. M.; Schelter, E. J.; Kuehl, C. J.; Clark, A. E.; Scott, B. L.; Morris, D. E.; Martin, R. L.; Thompson, J. D.; Kiplinger, J. L.; John, K. D. *Inorg. Chem.* **2005**, *44*, 5911−5920.
(4) Berg, D. J.; Boncella, J. M.; Andersen, R. A. *Organometallics* **2002**, *21*, 4622−4631.
(5) Carlson, C. N.; Kuehl, C. J.; Da Re, R. E.; Veauthier, J. M.; Schelter, E. J.; Milligan, A. E.; Scott, B. L.; Bauer, E. D.; Thompson, J. D.; Morris, D. E.; John, K. D. *J. Am. Chem. Soc.* **2006**, *128*, 7230−7241.
(6) Carlson, C. N.; Scott, B. L.; Martin, R. L.; Thompson, J. D.; Morris, D. E.; John, K. D. *Inorg. Chem.* **2007**, *46*, 5013−5022.
(7) Kuehl, C. J.; Da Re, R. E.; Scott, B. L.; Morris, D. E.; John, K. D. *Chem. Commun.* **2003**, 2336−2337.
(8) Schelter, E. J.; Veauthier, J. M.; Thompson, J. D.; Scott, B. L.; John, K. D.; Morris, D. E.; Kiplinger, J. L. *J. Am. Chem. Soc.* **2006**, *128*, 2198−2199.

10.1021/om061157o CCC: $37.00
Publication on Web 07/19/2007

Table 1. Model Structures of Bimetallic Ytterbocene Complexes and Precursors Based on Bridging Bis(bpy) and Bis(tpy) Motifs

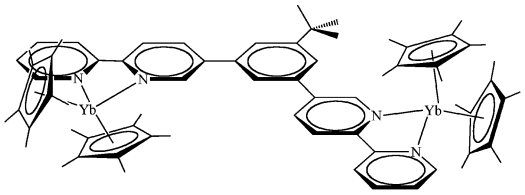

$[Cp^*_2Yb]_2$(*m*-bbb) (**1**)

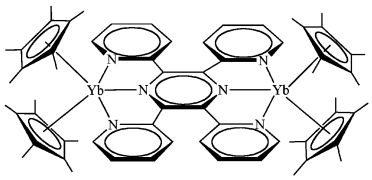

$[Cp^*_2Yb]_2$(tppz) (**4**)

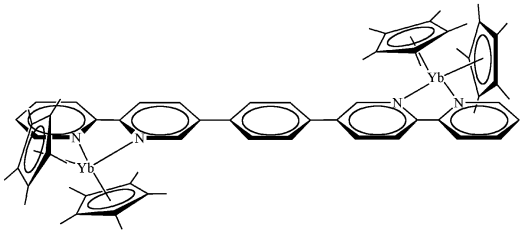

$[Cp^*_2Yb]_2$(*p*-bbb) (**2**)

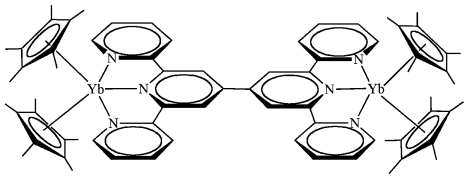

$[Cp^*_2Yb]_2$(qtp) (**5**)

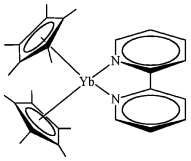

Cp^*_2Yb(bpy) (**3**)

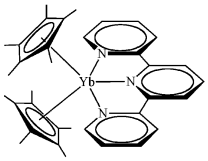

Cp^*_2Yb(tpy) (**7**)

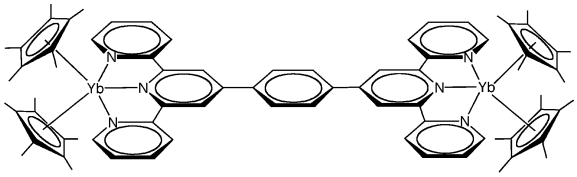

$[Cp^*_2Yb]_2$(*p*-dtb) (**6**)

preserve a higher-symmetry molecular axis between the metal centers while varying the metal−metal separation.[5,7] These systems were found to behave similarly to those of Andersen and co-workers in that the ytterbocene centers behave at higher temperatures as isolated Yb(III) species linked by a doubly reduced singlet polypyridyl dianion. Electronic communication between the metal centers (as evidenced by electrochemical data) was found to be most significant for the tppz-bridged bimetallic complex (**4**) that possesses the shortest metal−metal distance. In addition, the qtp-bridged bimetallic complex (**5**) was the only system to clearly exhibit evidence for antiferromagnetic superexchange coupling at low temperature. The stability of the singlet dianion electronic configuration on the bridging ligand is apparently a significant factor in determining the nature and extent of both the electronic and magnetic coupling in these systems.

We continue to pursue these multimetallic ytterbocene systems because of their potential to exhibit unusually large molecular magnetic moments and novel electronic properties since they can, in principle, possess both metal-based and bridging ligand-based spin carriers. The goal is to manipulate the coupling of spin carriers (metal and ligand) through the appropriate choice of bridging ligand symmetries and orbital energetics. The strategy pursued in the present report is to use a bridging bis(2,2′-bipyridyl) ligand framework to couple two ytterbocene centers, while varying the relative orientation of the bipyridyl moieties (and thus the ytterbocene groups) by changing the point of substitution on the phenyl ring used to link the bipyridyl groups from *meta*- to *para*-substituted (L = 1,3-(2,2′-bipyridyl)-5-^{t}Bu-C_6H_3 (*meta*-bis(bipyridyl)benzene; *m*-bbb) versus 1,4-(2,2′-bipyridyl)-C_6H_4 (*para*-bis(bipyridyl)benzene; *p*-bbb); Table 1). This novel polypyridyl bridging ligand system has been implemented in a similar vein in a recent investigation of the potential coupling of valence tautomers in bimetallic $Co^{III/II}$ dioxolene complexes.[9] However, in these Co dioxolene complexes the intramolecular redox partners (with the Co(III/II) redox couples) are the dioxolene ligands. The bis(bipyridyl) bridge serves to link the metal units and provide a potential through-bond π system to promote interaction. In contrast, in the bimetallic ytterbocene complexes, the bridging polypyridyl ligands are demonstrated to be primary participants in the intramolecular redox chemistry (with the Yb(III/II) couples). Thus, the bis(bipyridyl) systems should provide some direct insight into the role of bridging ligand π^* orbital energetics as well as intramolecular symmetry on determining the extent and magnitude of magnetic and electronic interactions. In fact, such paramagnetic metal/ligand radical interactions are key elements in the rapidly expanding field of molecular magnets.[10,11]

In this report we present synthesis and characterization (magnetic susceptibility, electrochemical, and electronic absorption spectroscopy) data for two new bimetallic ytterbocene complexes, $[Cp^*_2Yb]_2$(*m*-bbb) (**1**) and $[Cp^*_2Yb]_2$(*p*-bbb) (**2**), and their corresponding two-electron oxidation products, $[\mathbf{1}]^{2+}$ and $[\mathbf{2}]^{2+}$, and compare these results to those of the monometallic species Cp^*_2Yb(bpy) (**3**) and $[Cp^*_2Yb(bpy)]^+$ ($[\mathbf{3}]^+$) reported previously. The characterization data indicate that in both neutral bimetallic complexes the exchange coupling

(9) Bin-Salamon, S.; Brewer, S.; Depperman, E. C.; Franzen, S.; Kampf, J. W.; Kirk, M. L.; Lappi, S.; Kumar, R. K.; Preuss, K. E.; Shultz, D. A. *Inorg. Chem.* **2006**, *45*, 4461−4467.

(10) Miller, J. S.; Epstein, A. J. *Coord. Chem. Rev.* **2000**, *206*, 651−660.

(11) Koivisto, B. D.; Hicks, R. G. *Coord. Chem. Rev.* **2005**, *249*, 2612−2630.

mediated by the bis-2,2′-bipyridyl ligand is very small, with Yb−bpy interactions dominating the magnetic behavior of these complexes. Evidence for weak electronic interaction between the two $Cp^*_2Yb(bpy)$ centers in these bimetallic complexes derives from observed subtle changes in the optical spectroscopic data for the neutral complexes and differences in the spacing between the two metal-based reduction waves in the voltammetric data, for which the potential separation is greater in [**2**] than in [**1**]. The interpretation of these data is aided by theoretical calculations of the doubly reduced free ligands $(m\text{-bbb})^{2-}$ and $(p\text{-bbb})^{2-}$, suggesting that the spatially isolated diradical states are the lowest-lying states for these bridging ligands.

Experimental Section

Syntheses. All reactions and product manipulations were carried out under an atmosphere of dry argon or helium using standard drybox or Schlenk techniques. Anhydrous solvents, tetrahydrofuran (THF), toluene, and methylene chloride were purchased from Aldrich or Acros and stored in the glovebox over activated 4 Å molecular sieves overnight and passed the ketyl test before use. $Cp^*_2Yb{\cdot}OEt_2$[12] and $AgBPh_4$[13] were prepared according to the literature procedures. Ligands 1,3-(2,2′-bipyridyl)-5-^{t}Bu-C_6H_3 (*m*-bbb) and 1,4-(2,2′-bipyridyl)-C_6H_4 (*p*-bbb) were prepared as described previously.[9] Elemental analyses were performed by Midwest Microlab, Indianapolis, IN.

$(Cp^*_2Yb)_2$(*m*-bbb) (1). A room-temperature toluene solution (5 mL) of $Cp^*_2Yb{\cdot}OEt_2$ (128 mg, 0.24 mmol) was added to solid 1,3-bis(2,2′-bipyridine)-5-^{t}Bu-phenylene (54.8 mg, 0.12 mmol) with stirring. The solution immediately darkened and was stirred vigorously overnight. The following day, the toluene was removed under vacuum to yield a dark green powder (142 mg, yield 87%). Anal. Calcd for $C_{70}H_{86}N_4Yb_2$: C, 63.25; H, 6.48; N, 4.22. Found: C, 62.76; H, 6.47; N, 4.04. ^{1}H NMR (tol-d_8): δ 196.13 (s, *m*-bbb), 186.99 (s, *m*-bbb), 33.46 (s, *m*-bbb), 30.55 (s, *m*-bbb), 23.56 (s, *m*-bbb), 20.32 (s, *^{t}Bu*), 14.97 (s, *m*-bbb), 5.74 (s, C_5Me_5), −7.21 (s, *m*-bbb), −15.09 (s, *m*-bbb), −16.36 (s, *m*-bbb).

$(Cp^*_2Yb)_2$(*p*-bbb) (2). A room-temperature toluene solution (5 mL) of $Cp^*_2Yb{\cdot}OEt_2$ (111 mg, 0.22 mmol) was added to solid 1,4-bis(2,2′-bipyridine)phenylene (44.1 mg, 0.11 mmol) with stirring. The solution immediately darkened and was stirred vigorously overnight. The following day, the toluene was removed under vacuum to yield a dark green powder (112 mg, yield 81%). Anal. Calcd for $C_{66}H_{78}N_4Yb_2$: C, 62.26; H, 6.13; N, 4.40. Found: C, 62.28; H, 6.21; N, 4.39. ^{1}H NMR (tol-d_8): δ 46.29 (s, *p*-bbb), 26.53 (s, *p*-bbb), 19.51 (s, *p*-bbb), 16.71 (s, *p*-bbb), 14.76 (s, *p*-bbb), 6.22 (s C_5Me_5), −12.50 (s, *p*-bbb), −16.56 (s, *p*-bbb). Remaining *p*-bbb resonances are not observed presumably due to paramagnetic broadening or are obscured by solvent resonances.

$[(Cp^*_2Yb)_2(m\text{-bbb})][BPh_4]_2$ ($[1]^{2+}$). A room-temperature THF solution (5 mL) of $(Cp^*_2Yb)_2$(*m*-bbb) (53 mg, 0.04 mmol) was added to solid $AgBPh_4$ (33 mg, 0.08 mmol) with stirring in the dark. The solution was stirred vigorously overnight. The following day, the THF was removed under vacuum and the resulting powder was taken up into CH_2Cl_2 and filtered to yield a brown powder (69 mg, yield 89%). Anal. Calcd for $C_{118}H_{126}N_4B_2Yb_2{\cdot}3CH_2Cl_2$: C, 65.38; H, 5.99; N, 2.52. Found: C, 64.66; H, 5.91; N, 2.84. The slightly low carbon analysis is attributed to a partial occupancy (less than 3 molecules) of CH_2Cl_2 in the microcrystalline lattice. ^{1}H NMR (CD_2Cl_2): δ 93.94 (s, *m*-bbb), 57.91 (s, *m*-bbb), 46.85 (s, *m*-bbb), 42.61 (s, *tBu*), 20.58 (s, *m*-bbb), 9.15 (s, *m*-bbb), 6.97 (s, C_5Me_5), 6.75 (s, BPh_4), 6.28 (s, BPh_4), 6.00 (s, BPh_4), −13.13 (s, *m*-bbb), −15.52 (s, *m*-bbb). Resonances for the phenyl portion of *m*-bbb that were not observed are likely obscured by solvent peaks.

$[(Cp^*_2Yb)_2(p\text{-bbb})][BPh_4]_2$ ($[2]^{2+}$). A room-temperature THF solution (5 mL) of $(Cp^*_2Yb)_2$(*p*-bbb) (57.5 mg, 0.04 mmol) was added to solid $AgBPh_4$ (37.9 mg, 0.09 mmol) with stirring in the dark. The solution was stirred vigorously overnight. The following day, the THF was removed under vacuum and the resulting powder was taken up into CH_2Cl_2 and filtered to yield a brown powder (71.5 mg, yield 84%). Anal. Calcd for $C_{114}H_{118}N_4B_2Yb_2{\cdot}3CH_2Cl_2$: C, 64.86; H, 5.77; N, 2.59. Found: C, 64.70; H, 6.20; N, 3.25. ^{1}H NMR (CD_2Cl_2): δ 71.01 (s, *p*-bbb), 58.14 (s, *p*-bbb), 21.64 (s, *p*-bbb), 13.71 (s, *p*-bbb), 8.15 (s, BPh_4), 7.61 (s, C_5Me_5), 7.52 (s, BPh_4), 6.81 (s, BPh_4), −9.75 (s, *p*-bbb), −12.86 (s, *p*-bbb). Remaining *p*-bbb resonances are not observed presumably due to paramagnetic broadening or are obscured by solvent.

Magnetic Susceptibility. Magnetic susceptibility measurements over the temperature range 2 to 350 K were made using a Quantum Design superconducting quantum interference device (SQUID) magnetometer. The microcrystalline samples were sealed in borosilicate NMR tubes along with a small amount of quartz wool, which held the sample near the tube center. Contributions to the magnetization from quartz wool and tube were measured independently and subtracted from the total measured signal. The magnetic susceptibility, defined as the sample magnetization M divided by the applied magnetic field H, was measured as a function of temperature at an applied field of 0.1 T. Diamagnetic corrections were made using Pascal's constants.

Electrochemistry. Cyclic voltammetric studies were conducted in an inert atmosphere glovebox (nitrogen or helium) using a Perkin-Elmer Princeton Applied Research Corporation (PARC) model 263 potentiostat under computer control using M270 software. The electrochemical cell was either a modified PARC microcell consisting of a ∼3 mm platinum disc working electrode, a Pt wire counter electrode, and a silver wire quasi-reference electrode or a modified BAS microcell consisting of ∼1.5 mm Pt and Ag disc working and quasi-reference electrodes and a Pt wire counter electrode. All experiments were conducted in purified THF using ∼0.1 M $[(n\text{-}C_4H_9)_4N][B(C_6F_5)_4]$ as the supporting electrolyte. Measured potentials were calibrated using the ferrocene/ferrocenium couple. Data were analyzed using the IGOR Pro (Wavemetrics, Inc.) software package on a Macintosh platform.

Electronic Absorption Spectroscopy. Electronic absorption spectra from ∼200 to 2200 nm were recorded at room temperature using a Perkin-Elmer Lambda 19 spectrophotometer. Spectra were obtained in anhydrous THF (neutrals) and anhydrous CH_2Cl_2 (cations) against a solvent blank. All sample solutions were prepared and loaded into sealed quartz cells inside an inert atmosphere glovebox. Cells with 1 cm path length were used in the UV−visible region. However, for most NIR data, 1 mm path-length quartz cells were used to minimize contributions from solvent absorption band profiles. Typical slit widths were 2 nm in the UV−visible and 5−10 nm in the NIR.

Computational Methods. Calculations were carried out for neutral and doubly reduced ligands 1,3-(2,2′-bipyridyl)-5-CH_3-C_6H_3 (the 5-^{t}Bu was replaced by a CH_3 group to simplify calculations) and 1,4-(2,2′-bipyridyl)-C_6H_4 using the program Gaussian 03 (v. D.02)[14] utilizing the B3LYP hybrid density functional approach.[15,16] The 6-31G*(6d) basis set was used for all C, H, and N atoms.[17] The neutral ligand geometries were optimized and their vibrational frequencies calculated using analytic second derivatives. The neutral ligand structures were verified to be local minima with no imaginary

(12) Tilley, T. D.; Boncella, J. M.; Berg, D. J.; Burns, C. J.; Andersen, R. A. *Inorg. Synth.* **1990**, *27*, 146.
(13) Jordan, R. F.; Echols, S. F. *Inorg. Chem.* **1987**, *26*, 383−386.
(14) Frisch, M. J.; Trucks, G. W.; Schlegel, H. B.; et al. *Gaussian03*, Revision D.02; Gaussian, Inc.: Wallingford, CT, 2004.
(15) Lee, C.; Yang, W.; Parr, R. G. *Phys. Rev. B* **1988**, *37*, 785.
(16) Becke, A. D. *J. Chem. Phys.* **1993**, *98*, 5648−5652.
(17) Hehre, W. J.; Ditchfield, R.; Pople, J. A. *J. Chem. Phys.* **1972**, *56*, 2257−2261.

vibrations. The neutral geometries were employed to calculate the relative energies of the singlet dianion, singlet diradical, and triplet diradical electronic configurations.

Results and Discussion

General Synthesis. Complexes **1** and **2** were prepared by the reaction of 2 equiv of $Cp^*_2Yb(Et_2O)$ with 1 equiv of the appropriate bridging ligand, *m*-bbb or *p*-bbb, respectively, to provide dark green powders in good yield. ^{1}H NMR data support the expected ytterbocene-to-bridging ligand charge-transfer configuration given the large chemical shift window displayed by both **1** and **2**. The ^{1}H NMR spectrum of **1** exhibits only nine resonances associated with the *m*-bbb ligand. This suggests that the bpy moieties either are freely rotating about the bpy−phenylene bonds or are both locked into identical environments. The ^{1}H NMR spectrum of **2** appears to be similar to **1** in that it displays a number of ligand-based resonances indicative of a highly symmetric ligand geometry; however, it is missing at least one resonance. The missing resonance is likely one of the bpy protons in closest proximity to the Yb^{III} center; presumably it is not observed due to paramagnetic broadening. The dicationic forms of the complexes, $[\mathbf{1}]^{2+}$ and $[\mathbf{2}]^{2+}$, can be chemically isolated via addition of 2 equiv of $AgBPh_4$ to provide dark brown powders. Neither dicationic complex displays a full suite of bridging ligand resonances. Cationic complexes tend to provide better resolved resonances relative to the neutral analogues, so the missing signals are most likely obscured by the solvent or BPh_4^--based resonances. Repeated attempts were made to obtain single-crystal X-ray structures, but while crystals were isolated in all cases, none were found to be of diffraction quality.

Computational Chemistry. Previous investigations of neutral bimetallic ytterbocene complexes of bridging N-heterocyclic ligands have demonstrated the predominance of the singlet dianion electron configuration on the bridging ligand (i.e., $[(f)^{13}\text{-}(\pi^*)^2\text{-}(f)^{13}]$).[4,5,7] However, for bridging ligands consisting of bis-(polypyridyl) chelators linked by a phenyl group, the possibility exists to effectively uncouple the two polypyridyl chelators electronically by rotation about the phenyl−polypyridyl bonds, thereby spatially localizing low-lying π^* orbitals on the individual polypyridyl groups. Such torsional distortions were noted in the low-temperature crystal structures of both the *m*-bbb- and *p*-bbb-bridged Co dioxolene complexes, for which the bridging ligands are neutral (thus electron (de)localization is not an issue).[9] However, we obtained experimental evidence of the singlet dianion bridging ligand configuration in neutral bimetallic complexes **5** and **6** (Table 1) in solution,[5,7] even though these systems are both capable of a torsional distortion between the polypyridyl chelators that could disrupt the π^* orbital network and induce localization of the two added electrons into a diradical configuration. Thus, as a starting point in our consideration of the possible low-lying electronic configurations of these bis(bipyridyl)-bridged complexes, we turned to computations of the relative energies of the most probable electronic configurations on the doubly reduced bridging ligands. This presumes that each ytterbocene moiety will donate one electron to the bridging ligand in these systems, as seen in most other bimetallic ytterbocene complexes of polypyridyl ligands [4,5,7] and substantiated by the magnetic, spectroscopic, and electrochemical data presented below.

DFT calculations were performed on the bridging ligands 1,3-(2,2′-bipyridyl)-5-CH_3-C_6H_3 and1,4-(2,2′-bipyridyl)-C_6H_4 with the aim of determining the relative energies of the three most probable electronic states associated with the doubly reduced form of the bridging ligand: singlet dianion, singlet diradical, and triplet diradical. We readily acknowledge the limitations inherent in these calculations since they do not consider the potential perturbative influence of the two Cp^*_2Yb fragments on both steric and electronic properties of the bridging ligand, nor do they sample the many possible geometries available to these ligands. Our goal for this report is to a get an estimate of the relative energies of the differing electronic configurations for a stable ligand structural conformation. More detailed calculations for the complete bimetallic systems are underway and will be reported in a forthcoming contribution.

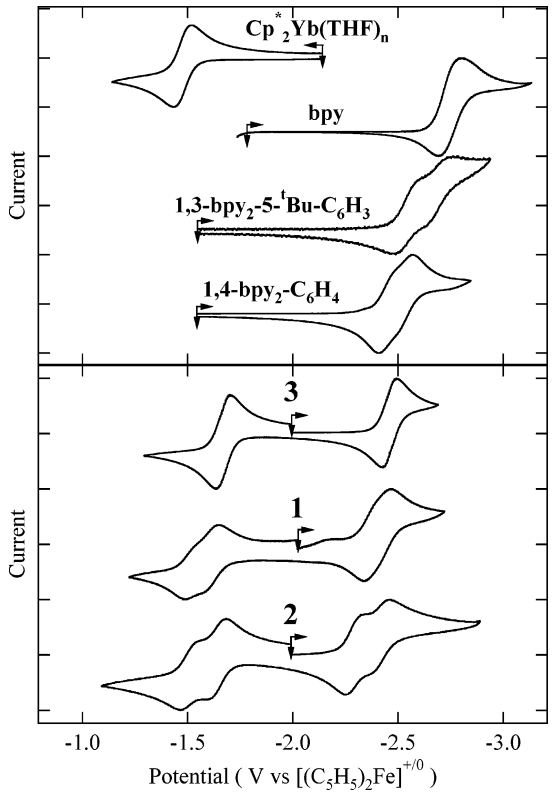

Figure 1. Cyclic voltammograms at a Pt disk working electrode in 0.1 M $[(n\text{-}C_4H_9)_4N][B(C_6F_5)_4]$/THF at room temperature. Scan rates were 200 mV/s. Concentrations of all analytes were ∼5 mM. Currents are in arbitrary units to facilitate comparisons. The vertical arrows indicate the rest potential for each system, and the horizontal arrows indicate the initial scan direction.

In the case of the 1,3-(2,2′-bipyridyl)-5-CH_3-C_6H_3 ligand, the triplet diradical state lies lowest, with the singlet diradical and singlet dianion lying 0.19 and 10.08 kcal above the triplet, respectively. In the case of the 1,4-(2,2′-bipyridyl)-C_6H_4 ligand, the singlet diradical lies lowest, with the triplet diradical and the singlet dianion lying 1.81 and 5.22 kcal higher in energy, respectively. Thus, the key outcome from these simple scoping calculations is that the singlet dianion state lies at substantially higher energy than either diradical state for both bridging ligands.

Electrochemistry. Room-temperature cyclic voltammograms for the free ligands, the ytterbocene precursor $Cp^*_2Yb(THF)_n$, and neutral complexes **1**−**3** in 0.1 M $[(n\text{-}C_4H_9)_4N][B(C_6F_5)_4]$/THF are presented in Figure 1. Metrical data extracted from these cyclic voltammograms are summarized in Table 2. The data for **3**, the uncomplexed bpy ligand, and the ytterbocene precursor have been reported by us previously,[1] but are reproduced here for comparison. The reversible oxidation wave for the ytterbocene THF adduct is attributed to the one-electron oxidation of the ytterbium metal center, $4f^{14} \rightarrow 4f^{13}$, as noted

Table 2. Summary and Comparison of Redox Data[a] for Ytterbocene Complexes

	ligand-based		metal-based		
ligand/complex	$E_{1/2}(L_1)$	$E_{1/2}(L_2)$	$E_{1/2}(M_a)$	$E_{1/2}(M_b)$	$\|\Delta(E_{1/2})[M - L]\|$[b]
bpy	−2.75				
3	−1.67		−2.46		0.79
1,3-bpy$_2$-5-^{t}Bu-C$_6$H$_3$	−2.55	−2.77			
1	−1.50	−1.63	−2.36	−2.45	0.73
1,4-bpy$_2$-C$_6$H$_4$	−2.44	−2.55			
2	−1.50	−1.66	−2.27	−2.43	0.61

	1,3-bpy$_2$-5-^{t}Bu-C$_6$H$_3$	**1**	1,4-bpy$_2$-C$_6$H$_4$	**2**
$\|\Delta(E_{1/2})[M_a - M_b]\|$		0.09		0.16
$\|\Delta(E_{1/2})[L_1 - L_2]\|$	0.22	0.13	0.11	0.16

[a] All values in volts. $E_{1/2}$ values are versus $[(C_5H_5)_2Fe]^{+/0}$ in 0.1 M $[(n\text{-}C_4H_9)_4N][B(C_6F_5)_4]$/THF at room temperature. [b] Separation in $E_{1/2}$ values between most positive metal-based reduction wave and most negative ligand-based oxidation wave.

previously.[1] Note that in the uncomplexed form both bridging bipyridyl-based ligands (*m*-bbb and *p*-bbb) exhibit two poorly resolved, but reversible reduction waves within the available potential window of this solvent/supporting electrolyte system. These reduction processes in the free ligands are clearly associated with two successive one-electron additions into the low-lying π^* orbital(s). However, it is unclear in this case whether both electrons enter the same orbital (delocalized over the entire ligand framework) to give $(\pi^*)^1$ and $(\pi^*)^2$ electronic configurations, respectively, or whether there are two nearly degenerate low-lying π^* orbitals (due, for example, to disruption of an extended π^* orbital from torsions about the bridging phenyl group) that each accept one electron. The spacing between these two reduction waves for *m*-bbb (220 mV, Table 2) is comparable to that observed in the phenyl-bridged bis(terpyridyl) ligand (*p*-dtb).[5] However, the spacing between the two waves in *p*-bbb is only 110 mV, approaching the value expected for two noninteracting redox centers.[18] The spacing between waves in both bis(bpy) systems is significantly smaller than expected for occupation of two electrons in the same orbital (the dianion configuration) since in this case the spacing would correspond approximately to a spin pairing energy and is typically ∼1 V.[19] The DFT result described above suggests that the diradical state lies lowest for both these ligands. This would be consistent with an interpretation of the voltammetric data as populating two nearly degenerate orbitals, with the interaction being slightly larger in the *m*-bbb system than the *p*-bbb system.

For the bimetallic complexes, **1** and **2**, there are two reduction waves and two oxidation waves observed in the potential region from ∼0 to −3.0 V vs $[Cp_2Fe]^{+/0}$ (Figure 1). Additional irreversible voltammetric waves are also seen at ca. +1 V and more negative than −3 V vs $[Cp_2Fe]^{+/0}$. The former are attributed to oxidation of the Cp* ligands as noted previously,[1,20] and the latter are believed to be further polypyridyl ligand-based reductions. The four waves shown for **1** and **2** (Figure 1) are all chemically reversible one-electron processes.

Our previous studies of the electrochemical properties of these polypyridyl adducts of ytterbocene (including **3**)[1,3,5,7] establish the basis for assignment of the four reversible redox waves in **1** and **2**. Specifically, for **3** the voltammetric waves are ascribed to a metal-based one-electron reduction step ($4f^{13} \rightarrow 4f^{14}$) and a ligand-based one-electron oxidation step ($bpy^{\bullet -} \rightarrow bpy^0$).[1] Similarly, the voltammetric waves for **1** and **2** in Figure 1 can be ascribed to two successive one-electron oxidations of the bridging ligand and a one-electron reduction of each of the two ytterbium metal centers. This same general pattern was exhibited by all the tpy-based bimetallic complexes (**4**−**6**), although the spacings between the waves were substantially larger for some of the tpy-based bimetallic complexes.[5]

The potential separation between waves is one of the most important diagnostic aspects of these voltammetric data, as it provides direct information on the degree of electronic interaction between the metal centers and between each metal center and the bridging ligand. These data are all summarized in Table 2. The most salient parameter to assess the electronic interactions is the potential separation between the waves associated with the metal-based processes ($\Delta(E_{1/2})[M_a - M_b]$ in Table 2). While this metric has been shown recently to be sensitive to ion-pairing and solvation effects,[21−24] and can be varied significantly by changing the solvent/supporting electrolyte composition, we have kept the solvent/supporting electrolyte system (THF/∼0.1 M $[(n\text{-}C_4H_9)_4N][B(C_6F_5)_4]$) constant throughout the studies reported here and previously.[1,3,5,7] Thus, comparisons of $\Delta(E_{1/2})$ values among these ytterbocene complexes remain strictly valid and informative of *differences* in the extent of electronic communication in a relative sense among these systems.

In the absence of any metal−metal interaction, the metal-based redox processes should occur at the same potential (i.e., two superimposed one-electron waves) with perhaps a slight, experimentally indiscernible offset (∼36 mV) due to statistical (entropic) factors.[18] The actual value for **1** (90 mV) is approaching this theoretical limit, demonstrating that the electronic interaction between metals is essentially negligible. The value for **2** (160 mV) is comparable to that observed for the *para*-substituted tpy-based dimer (*p*-dtb; 220 mV [5]), indicating some weak interaction between the metal centers in **2**. (For comparison, this value is 600 mV in the more strongly interacting tppz-based bimetallic complex **4**.)[5]

The separation between the bridging-ligand-based oxidation waves ($\Delta(E_{1/2})[L_1 - L_2]$ in Table 2) for the bimetallic complex **1** (130 mV) is actually smaller that that observed for the free *m*-bbb ligand reduction processes (220 mV), whereas this value for **2** increases slightly (160 mV) relative to the value for free *p*-bbb (110 mV). Nonetheless, these wave spacings for the ligand-based redox processes in the ytterbocene complexes are quite similar to those for the uncomplexed ligands. As noted

(18) Bard, A. J.; Faulkner, L. R. *Electrochemical Methods: Fundamentals and Applications*; John Wiley and Sons: New York, 2001.
(19) Vlcek, A. A. *Coord. Chem. Rev.* **1982**, *43*, 39−62.
(20) Morris, D. E.; Da Re, R. E.; Jantunen, K. C.; Castro-Rodriguez, I.; Kiplinger, J. L. *Organometallics* **2004**, *23*, 5142−5153.
(21) Barriere, F.; Camire, N.; Mueller-Westerhoff, U. T.; Sanders, R. *J. Am. Chem. Soc.* **2002**, *124*, 7262−7263.
(22) Barriere, F.; Geiger, W. E. *J. Am. Chem. Soc.* **2006**, *128*, 3980−3989.
(23) D'Alessandro, D. M.; Keene, F. R. *Dalton Trans.* **2004**, 3950−3954.
(24) Yeomans, B. D.; Kelso, L. S.; Tregloan, P. A.; Keene, F. R. *Eur. J. Inorg. Chem.* **2001**, 239−246.

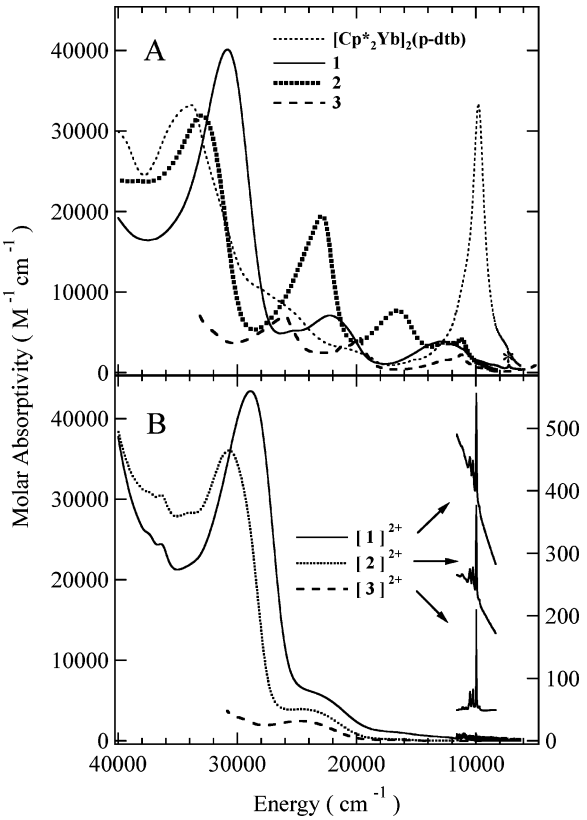

Figure 2. UV−vis−near-IR electronic absorption spectra in THF (A, neutrals) or CH_2Cl_2 (B, dications) at 300 K. The spectrum of $[Cp^*_2Yb]_2$(*p*-dtb) (**6**) in THF has been included in A for comparison. The spectral feature marked with an asterisk in A is an uncorrected solvent overtone vibrational band.

above, this behavior is most consistent with the diradical ligand electronic configuration $((\pi_A^*)^1(\pi_B^*)^1)$ such that, in **1** and **2**, the oxidation waves correspond to removal of electrons from nearly degenerate but distinct orbitals.

Optical Spectroscopy. The room-temperature UV−visible−near-IR electronic absorption spectral data for neutral complexes **1** and **2** in THF and dications $[\mathbf{1}]^{2+}$ and $[\mathbf{2}]^{2+}$ in CH_2Cl_2 are provided in Figure 2. Previously reported data for the monometallic species **3** and $[\mathbf{3}]^+$ are included for comparison.[1] Because of the large number of possible electronic transitions in both the neutral and cationic complexes, detailed band assignments of the observed optical transitions are outside of the scope of this effort. Instead we focus on a comparison of the spectral properties for **1**, **2**, and **3** and those of their respective (di)cations, particularly in relation to the behavior observed and reported previously for the tpy-based bimetallic systems.[5]

Neutral Complexes. The optical spectral data for the neutral complexes (Figure 2A) show a generally good correspondence in the number, energy, and intensity of the bands across the three complexes. Each complex possesses a series (3 or 4) of vibronically structured bands of moderate to high intensity that spans the near-ultraviolet and visible regions of the spectra. The intensities suggest that these electronic transitions are electric dipole allowed, and the bandwidths and varying degrees of vibronic structure indicate that there are Frank−Condon-active vibrational modes coupled to these electronic states. One of the most significant aspects of the spectra for **1** and **2** is the *absence* of the very intense, narrow, vibronically structured band seen previously in the spectra of all tpy-based bimetallic neutral complexes (**4**−**6**) at ∼10 000 cm^{-1} (illustrated for the bimetallic *p*-dtb complex **6** in Figure 2A).[5] This transition has been assigned to the lowest energy $\pi^*-\pi^*$ transition (i.e., promotion of an electron from the highest doubly occupied π^* orbital in the dianion to the lowest unoccupied π^* orbital) in the singlet dianion bridging ligand in the tpy-based bimetallic complexes, and it is the hallmark electronic spectral signature for the singlet dianion electronic configuration.[25−28] Thus, the absence of this transition in **1** and **2** indicates that these systems do not possess singlet dianion bridging ligands, consistent with the results from DFT calculations and electrochemical data on ligand-based redox processes discussed above. The other noteworthy aspect of the data for **1** and **2** is the strong similarity they bear to the data for the monometallic neutral complex **3**. The electronic transitions in this spectral region in **3** have been assigned previously to bpy−radical anion based $\pi-\pi^*$ and $\pi^*-\pi^*$ transitions.[1] This similarity is in stark contrast to the behavior of the tpy-based bimetallic systems (**4**−**6**), in which the spectra of the neutral species bear no resemblance to that of Cp^*_2Yb(tpy) (**7**).[5] Thus, the two most significant observations from the spectral data for the neutral complexes together indicate that (1) the bridging ligand does not possess a simple $(\pi^*)^2$ electronic configuration and (2) the electronic properties of the bimetallic systems appear closer to a simple superposition of two monometallic ytterbocene moieties.

Unfortunately, the optical data for **1** and **2** show no evidence for the f−f electronic bands expected for systems containing Yb(III) ions. These bands should provide a key diagnostic for electronic and/or magnetic coupling between the metal centers, but they are expected to lie at ∼10 000 cm^{-1} (vide infra), and the comparatively low oscillator strengths derived from their parity-forbidden character makes them indiscernible beneath the more intense ligand radical transitions that tail into this spectral window. These diagnostic bands have been absent from the spectra of nearly all neutral ytterbocene polypyridine adducts we have investigated.[1,3,5,7] There is, however, some suggestion of a difference in the electronic interaction(s) between the two Cp^*_2Yb(bpy) moieties in **1** versus **2** in these spectral data. In particular, the band maxima for **2** appear to be red-shifted by ∼1000−2000 cm^{-1} relative to those of **1** (assuming a band correlation in the spectra for **1** and **2** in the three highest energy bands). If, as most data suggest, the ground electronic state in both **1** and **2** can be described as effectively possessing two independent $Yb^{III}/bpy^{-\bullet}$ chromophores, this spectral difference likely reflects a difference in the $\pi-\pi^*$ and $\pi^*-\pi^*$ excited states of the two systems (i.e., there is a dissimilarity in the LUMO energies of these ligand diradicals as intimated by the DFT results).

Cationic Complexes. The optical data for $[\mathbf{1}]^{2+}$, $[\mathbf{2}]^{2+}$, and $[\mathbf{3}]^+$ over the entire UV−vis−NIR spectral range are provided in Figure 2B. These spectral data are significantly simplified relative to the neutral complex data because these species no longer possess electrons in polypyridyl-based π^* orbitals that engender the intense transitions throughout the visible and NIR spectral regions. However, as observed for the neutral complexes, there is a high degree of correlation among these spectra in terms of the number, energy, and intensity of the transitions. The correlation is arguably even better for the cationic complexes than for the neutrals, but the spectra of the dications also

(25) Bachmann, R.; Gerson, F.; Gescheidt, G.; Vogel, E. *J. Am. Chem. Soc.* **1992**, *114*, 10855−10860.
(26) Bachmann, R.; Gerson, F.; Gescheidt, G.; Vogel, E. *J. Am. Chem. Soc.* **1993**, *115*, 10286−10292.
(27) Mack, J.; Stillman, M. J. *Inorg. Chem.* **1997**, *36*, 413−425.
(28) Kenny, P. W.; Jozefiak, T. H.; Miller, L. L. *J. Org. Chem.* **1988**, *53*, 5007−5010.

reveal a slight red-shift (~2000 cm^{-1}) of the observed visible bands of $[\mathbf{2}]^{2+}$ relative to those of $[\mathbf{1}]^{2+}$. The assignments for these bands are identical to those proposed previously for cationic monometallic and dicationic bimetallic ytterbocene complexes.[1,3,5,7,29] Specifically, the most intense resolved transitions for $[\mathbf{1}]^{2+}$and $[\mathbf{2}]^{2+}$ at energies greater than ~26 000 cm^{-1} are assigned to $\pi-\pi^*$ transitions localized on the polypyridyl and Cp* ligands. There are two additional unique features common to the spectra of all these cationic species. The first is the set of two (or more) broad bands with spectral centers that occur in the mid-visible region: the higher-energy component at ~23 000−24 000 cm^{-1} and the lower-energy component at ~16 000−18 000 cm^{-1}. The higher energy, more intense of these bands is assigned to a polypyridyl ligand (π)-to-metal (4f) charge-transfer transition on the basis of detailed resonance Raman data for $[\mathbf{3}]^{+}$ presented elsewhere [29] and by analogy with the spectrum of oxidized (d^5) transition-metal polypyridyl complexes (e.g., $[Ru(bpy)_3]^{3+}$).[30−33] The less intense band(s) in this region are assigned to the related Cp* ligand (π)-to-metal (4f) charge-transfer transition(s). This assignment is based on comparison to the spectra of many structurally related monometallic ytterbocene complexes (e.g., Cp^*_3Yb and $Cp^*_3Yb(L)$; L = THF, PEt_3, etc.).[34] The second new feature for these dicationic species (and $[\mathbf{3}]^{+}$) is the emergence of the f−f transitions deriving from the f^{13} electronic configuration on the two ytterbium (one for $[\mathbf{3}]^{+}$) centers (right-hand scale, Figure 2B). As expected on the basis of data from other Yb(III) complexes, these bands are centered at ~10 000 cm^{-1}, they are quite narrow, and they have much lower oscillator strengths, consistent with the Laporte-forbidden nature of the transitions.

To examine in greater detail the comparative properties of the f−f bands in these three species, the contribution to the f−f region from the sloping low-energy tail of the charge-transfer bands in $[\mathbf{1}]^{2+}$ and $[\mathbf{2}]^{2+}$ was eliminated by fitting the charge-transfer band envelope to a Gaussian profile and subtracting this profile from the f−f ligand field region of the spectrum. Figure 3 shows the energy and intensity comparison of the f−f spectral region for the three cationic complexes. Note, in particular, the striking similarity in the spectra of all three complexes in peak positions and intensities. To quantify this comparison, the spectra in this region for all three species were fit using Voigt functions.[35] (Either pure Gaussian or pure Lorentzian profiles were totally inadequate.) The fitting results are included in the traces in Figure 3, and the metrical results for each of the required six spectral bands identified in Figure 3 are provided in Table 3. (One additional band at 10 120 cm^{-1} was required to fit the full spectral envelope for $[\mathbf{1}]^{2+}$.) Note that the energies of the peak maxima and the integrated intensities in the band for each of the six bands are very nearly identical for each of the three spectra.

The properties of these f−f ligand field spectra, and specifically the comparison of the data for bimetallic species $[\mathbf{1}]^{2+}$ and $[\mathbf{2}]^{2+}$ versus the monometallic species $[\mathbf{3}]^{+}$, should reflect in some way the extent of the electronic interaction and potentially even the exchange coupling interaction between the metal centers in the bimetallic systems.[36,37] Potential spectral signatures of these interactions include simultaneous pair excitations at approximately twice the energy of the single-ion absorptions, band splittings, and intensity enhancements. All of these effects have been observed previously in multimetallic Yb(III) systems, but all reports have been for solid-state species such as oxides and ternary halides.[38,39] We know of no published reports making the direct comparison of f−f spectral data for

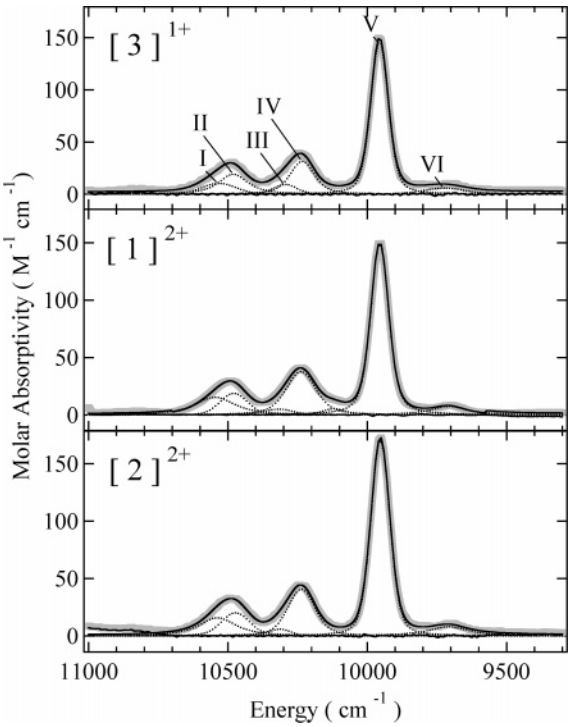

Figure 3. Baseline-corrected near-IR spectral data for fully oxidized ytterbocene dication complexes in CH_2Cl_2. Data are thick gray lines; unconstrained Voigt function fits are solid black lines; individual band components from fits are dashed lines.

Table 3. Summary of f−f Spectral Data from NIR Spectra of Cationic Ytterbocene Complexes

		complex		
spectral band[a]		$[\mathbf{1}]^{2+}$	$[\mathbf{2}]^{2+}$	$[\mathbf{3}]^{+}$
I	energy (cm^{-1})	10 546	10 537	10 532
	intensity[b]	3780	3680	1650
II	energy (cm^{-1})	10 479	10 473	10 481
	intensity	2410	2840	3470
III	energy (cm^{-1})	10 318	10 313	10 295
	intensity	790	600	1040
IV	energy (cm^{-1})	10 238	10 237	10 233
	intensity	6070	5820	4270
V	energy (cm^{-1})	9955	9953	9956
	intensity	14430	16230	13250
VI	energy (cm^{-1})	9707	9709	9723
	intensity	1800	2160	1320

[a] See Figure 3 for identification of bands. [b] Integrated intensities (arb. units) are derived from the unconstrained Voigt profile fits of the spectra (ref 35); see text for details.

(29) Da Re, R. E.; Kuehl, C. J.; Donohoe, R. J.; John, K. D.; Morris, D. E. *Electronic Spectroscopy of [(C_5Me_5)$_2$Yb(L)]$^+$ (L=2,2′-bipyridine and 2,2′:6′,2″-terpyridine). Vibronic Coupling and LIgand-Field Splitting in the $4f^{13}$-Derived Ground and Excited States of Yb^{3+}*; Los Alamos National Laboratory: Los Alamos, NM, 2005; LA-UR-05-5249.

(30) Bergkamp, M. A.; Gutlich, P.; Netzel, T. L.; Sutin, N. *J. Phys. Chem.* **1983**, *87*, 3877−3883.

(31) Braterman, P. S.; Song, J. I.; Peacock, R. D. *Spectrochim. Acta, Part A* **1992**, *48*, 899−903.

(32) Bryant, G. M.; Fergusson, J. E. *Aust. J. Chem.* **1971**, *24*, 275−286.

(33) Nazeeruddin, M. K.; Zakeeruddin, S. M.; Kalyanasundaram, K. *J. Phys. Chem.* **1993**, *97*, 9607−9612.

(34) Schlesener, C. J.; Ellis, A. B. *Organometallics* **1983**, *2*, 529−534.

(35) Armstrong, B. H. *J. Quant. Spectrosc. Radiat. Transfer* **1967**, *7*, 61−88.

(36) McCarthy, P. J.; Gudel, H. U. *Coord. Chem. Rev.* **1988**, *88*, 69−131.

(37) Tuczek, F.; Solomon, E. I. *Coord. Chem. Rev.* **2001**, *219*, 1075−1112.

(38) Hehlen, M. P.; Gudel, H. U. *J. Chem. Phys.* **1993**, *98*, 1768−1775.

(39) Schugar, H. J.; Solomon, E. I.; Cleveland, W. L.; Goodman, L. *J. Am. Chem. Soc.* **1975**, *97*, 6442−6450.

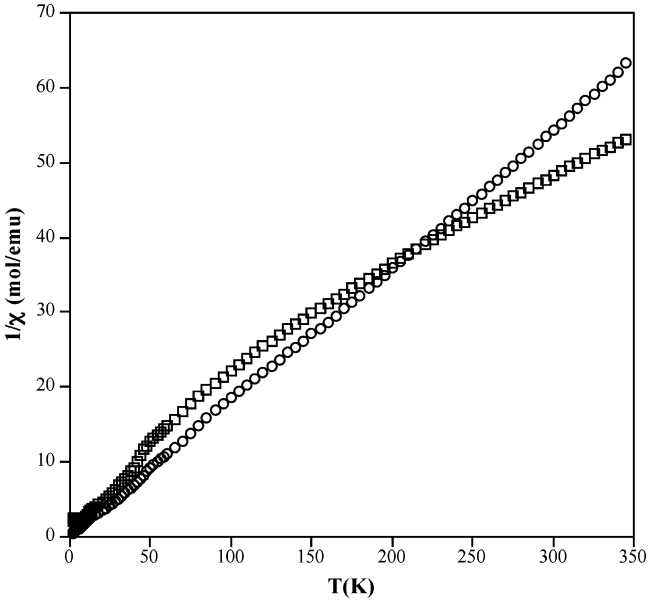

Figure 4. $1/\chi$ vs T for $[(Cp^*_2Yb)_2BL][BPh_4]_2$ at 0.1 T. BL = *m*-bbb (○) and *p*-bbb (□).

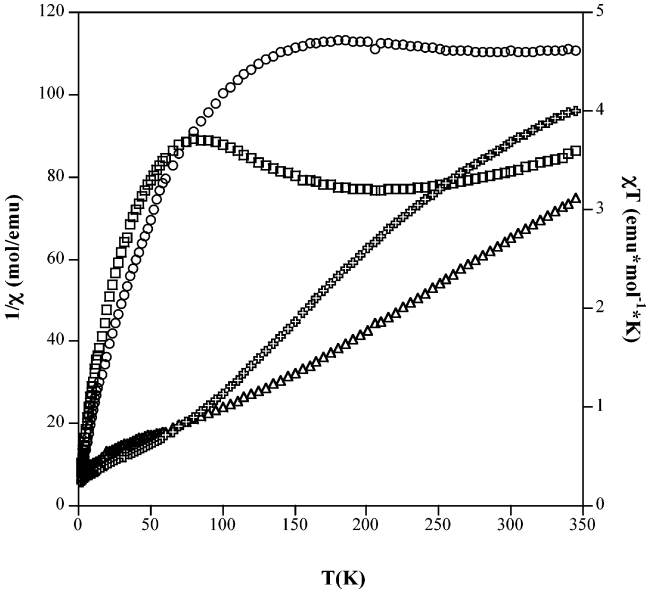

Figure 5. $1/\chi$ (○,□) and χT (▲,+) vs T for $(Cp^*_2Yb)_2BL$ at 0.1 Tesla. BL = *m*-bbb (○,▲) and *p*-bbb (□,+).

structurally homologous single-molecule monometallic versus bimetallic lanthanide or actinide complexes.

In our previous studies of the tpy-based ytterbocene multimetallic systems (**4**−**6**) in comparison to the monometallic ytterbocene tpy adduct (**7**), we did observe some significant perturbations in the f−f ligand field region for the three bimetallic dicationic complexes relative to monometallic cation. These perturbations ranged from complete alteration in position and intensity of the bands for the most strongly interacting system (**4**) to small (unresolved) splittings of bands and increases in band intensities for the more weakly interacting systems (**5** and **6**).[5] Clearly the data in Figure 3 and Table 3 indicate no such perturbations in these bpy-based bimetallic systems. As was the case for the neutral bimetallic complexes described above, the only optical spectral datum that reflects a difference in behavior is the slight red-shift in the intensities of the charge-transfer bands, and this is most likely a consequence of the nature of the bridging ligand LUMO in $[\mathbf{2}]^{2+}$ versus $[\mathbf{1}]^{2+}$. We cannot rule out the presence of simultaneous pair excitation transitions in these systems for either the neutrals or the dications because, like the single-ion f−f excitations in the neutral complexes discussed above, the ligand-based and charge-transfer transitions in the anticipated region of these pair excitations ($\sim$20 000 cm^{-1}) would obscure the presence of the much weaker pair excitation transitions.

Magnetic Susceptibility. Magnetic susceptibility data for compounds $[\mathbf{1}]^{2+}$, $[\mathbf{2}]^{2+}$, **1**, and **2** are presented in Figures 4 and 5. The initial interpretation of the magnetic data is based on the premise that the electronic configuration for the dicationic species is $[(f)^{13}\text{-}(\pi^*)^0\text{-}(f)^{13}]$, as seen in previously studied bimetallic ytterbocene complexes.[4,5] On the basis of DFT results and electrochemical and optical spectroscopic data described above, the electronic configuration for the neutral species is presumed to be $[(f)^{13}\text{-}(\pi_a^*)^1\text{-}(\pi_b^*)^1\text{-}(f)^{13}]$. However, this configuration can still give rise to a number of different magnetic exchange coupling schemes as described below. The magnetic data for $[\mathbf{1}]^{2+}$ and $[\mathbf{2}]^{2+}$ (Figure 4) reveal room-temperature moments (μ_{eff}) of 6.65 and 7.04 μ_β (or BM), respectively. The predicted effective magnetic moment (μ_{eff}) in the high-temperature limit for two uncoupled Yb^{III} ions is 6.4 μ_β.[4]

Unlike the case for the dicationic species, the χ^{-1} versus T plots for the neutral complexes **1** and **2** (Figure 5) depart dramatically from the Curie law and exhibit a temperature-dependent profile reminiscent of monometallic analogues such as $Cp^*_2Yb(L)$ (L = bpy,[2] tpy,[3] and 4′-CN-tpy[3]). We had previously ascribed this type of temperature-dependent behavior to a valence tautomeric (VT) equilibrium[40−43] between the magnetic $(f)^{13}\text{-}(\pi^*)^1$ and nonmagnetic $(f)^{14}\text{-}(\pi^*)^0$ forms of the monometallic complex. However, recent variable-temperature electronic absorption spectral data obtained for $Cp^*_2Yb(tpy)$ in a polymer film matrix suggest that a tautomeric equilibrium does not exist in these systems.[44] In particular, the spectrum obtained at 30 K looks identical to that seen at 270 K (where the magnetic $(f)^{13}\text{-}(\pi^*)^1$ form is known to be the principal species) except for the slight line-narrowing in the bands anticipated for the lower-temperature conditions (see Figure S1 in Supporting Information). Thus, the temperature-dependent magnetic behavior observed for **1** and **2** must be ascribed to variations in the thermal population of ligand-field split Kramers doublets within the $^2F_{7/2}$ manifold of the Yb(III) centers, lanthanide−radical exchange coupling, radical−radical exchange coupling, or a combination of these factors.

The χT versus T data for **1** and **2** are also shown in Figure 5. Under the assumption that the bridging ligand in these neutral complexes is best described as a diradical possessing two spatially isolated spins, there are three possible exchange interactions in **1** and **2** to consider; two are equivalent ($J_{f-\pi}$) and describe magnetic interactions between the f^{13} Yb^{3+} ion and the diimine radical anion and the third ($J_{\pi-\pi}$) describes the nature of the exchange between the two radical anion diimine ligands. There are a number of *limiting* cases involving the ratio of the two independent exchange interactions (note: $J < 0$ indicates an antiferromagnetic interaction, while $J > 0$ indicates a ferromagnetic interaction). These are summarized in Table 4 and discussed below in light of the experimental data.

Cases 1, 4, 5, and 8 may immediately be ruled out, as these possess nonmagnetic ($\boldsymbol{J} = 0$, where $\boldsymbol{J} = \boldsymbol{L} + \boldsymbol{S}$) ground states.

(40) Hendrickson, D. N.; Pierpont, C. G. *Topics in Current Chemistry*; Springer-Verlag: Berlin, 2004.
(41) Pierpont, C. G. *Coord. Chem. Rev.* **2001**, *216*, 99−125.
(42) Pierpont, C. G. *Coord. Chem. Rev.* **2001**, *219*, 415−433.
(43) Shultz, D. A. *Magnetism: Molecules to Materials II: Molecule-Based Materials*; Wiley-VCH: Weinheim, Germany, 2002.
(44) Rubie, N.; Knottenbelt, S. Z.; Kirk, M. L. Manuscript in preparation.

Table 4. Limiting Cases for Magnetic Coupling in a Four-Spin Doubly-Reduced Bridging Ligand (L) Bimetallic System with Spatially Isolated Bridging Ligand Electrons

	Coupling Scheme[a]		Relative Coupling Magnitude	Schematic Representation	Ground State
Case	$\pi-\pi$	$f-\pi$	$\lvert J_{\pi-\pi}\rvert$ vs. $\lvert J_{f-\pi}\rvert$	M_a L M_b	
1	A	A	>	↓ ↑↓ ↑	J = 0
2	F	F	>	↑ ↑↑ ↑	J ≠ 0
3	F	A	>	↓ ↑↑ ↓	J ≠ 0
4	A	F	>	↑ ↑↓ ↓	J = 0
5	A	A	<	↑↓ ↑↓	J = 0
6	F	F	<	↑↑ ↑↑	J ≠ 0
7	F	A	<	↑↓ ↓↑	J ≠ 0
8	A	F	<	↑↑ ↓↓	J = 0
9	~0	A/F	<<	↕↕ ↕↕	J ≠ 0
10	A/F	~0	>>	↕ ↕↕ ↕	J ≠ 0

[a] A = antiferromagnetic; F = ferromagnetic.

The large magnetic moments predicted for the ground states in cases 2 and 6 are inconsistent with the observed data and preclude these as viable possibilities. Marked differences in the susceptibility for **1** versus **2** due to the different linkage isomerism (*meta* vs *para*) are expected whenever $|J_{\pi-\pi}| > |J_{f-\pi}|$ (cases 3 and 10). Thus, since the low-temperature magnetic behavior is very similar for both **1** and **2**, we can eliminate cases 3 and 10. As such, the best explanations lie with cases 7 and 9. In case 7 $|J_{f-\pi}| > |J_{\pi-\pi}|$, while for case 9 $J_{\pi-\pi} \approx 0$ (i.e., $|J_{\pi-\pi}| \ll |J_{f-\pi}|$). Note that the magnetic properties for both cases are dominated by the nature of the Yb^{3+}−ligand radical exchange, $J_{f-\pi}$. This would result from a poor spin delocalization onto the phenyl bridge fragment due to inherently poor electronic communication across the 1,3/1,4-(2,2′-bipyridyl)-C_6H_4 unit and/or substantial ring torsions (θ) about the bpy−Ph bonds, the latter of which would result in a $\cos^4\theta$ modulation of $J_{\pi-\pi}$.[45] Elucidating the sign and magnitude of $J_{f-\pi}$ in this limit is complicated due to the presence of trace magnetic impurities leading to Curie tails and potential subtle differences in ligand field effects. Magnetic circular dichroism spectroscopy studies are currently underway in an attempt to improve the description of the ground-state magnetic behavior and the nature of $J_{f-\pi}$ in these neutral complexes.

Summary and Conclusions

The electrochemical, optical, and magnetic susceptibility characterization data presented herein for the two new bimetallic complexes, $[Cp^*_2Yb]_2$(*m*-bbb) (**1**) and $[Cp^*_2Yb]_2$(*p*-bbb) (**2**), and their corresponding two-electron oxidation products, $[\mathbf{1}]^{2+}$ and $[\mathbf{2}]^{2+}$, together with the theoretical calculations for the uncomplexed ligands *m*-bbb and *p*-bbb provide a coherent description of the electronic structure of these systems that is best described as an $[(f)^{13}\text{-}(\pi_A^*)^1\text{-}(\pi_B^*)^1\text{-}(f)^{13}]$ configuration for which the bridging polypyridyl ligands support two effectively independent radical anions. Consistent with this description, there is only weak electronic coupling between the two Yb^{III} metal centers in the neutral and oxidized species, and magnetic exchange coupling in the neutral complexes is limited to the interactions between each Yb^{III} center and its associated ligand radical. This behavior is in contrast to that observed for the analogous bridging bis(tpy) bimetallic ytterbocene complexes (**4**−**6**) that were all found to exist in a dianionic bridging ligand configuration ($[(f)^{13}\text{-}(\pi^*)^2\text{-}(f)^{13}]$) with evidence for greater electronic and, at least for **5**, magnetic coupling between the metal centers.[5,7]

The striking similarity in the electronic and magnetic behavior of **1** and **2** was not anticipated. In particular, the fact that **2** does not display behavior similar to that of the linear bis(tpy) bridging ligand systems was surprising inasmuch as the 1,4-substitution pattern on the phenyl linker could in principle promote spin-pairing of the two bridging ligand electrons and induce antiferromagnetic coupling between the metal centers. However, the overall low symmetry of these complexes as a result of the conformation of the phenyl bridge relative to the bpy rings and the potential for torsional distortions about the bpy−C_6H_4 bonds suggest that they are likely predisposed to spin localization on the bpy orbital framework that severely attenuates both electronic and magnetic communication along the vector(s) connecting the metal centers. This exchange modulation as a function of bridging ligand conformation has been documented with semiquinone-type dinuclear complexes.[46−48] It is noteworthy that this same bridging ligand set (*m*-bbb versus *p*-bbb) was found to engender different behavior in bimetallic $Co^{III/II}$ dioxolene complexes.[9] In the Co systems the *p*-bbb ligand was determined to promote greater magnetic coupling than the *m*-bbb ligand, although the electronic interactions (as evidenced by the intervalence charge-transfer transitions) were comparable for both ligand sets. However, this difference in behavior between the Yb and Co bimetallic systems may simply be a manifestation of the occupancy of antibonding orbitals on the bridging ligands in the former systems that drive structural distortions of the ligands inducing localization of spin carriers. Future studies will focus upon the use of magnetic circular dichroism (MCD) spectroscopy in an attempt to improve the description of the magnetic behavior of these neutral complexes at low temperature. Furthermore, other ligand frameworks (e.g., the 1,3-analogue of the previously studied 1,4-di(4′-terpyridyl)benzene (dtb) bimetallic ytterbocene complex[6]) have been synthesized to further explore the effects of bridging ligand connectivity on the magnetic/electronic properties of these materials.

Acknowledgment. Funding for this work was provided by Los Alamos National Laboratory's Laboratory Directed Research and Development program and by the U.S. Department of Energy, Office of Basic Energy Sciences, under the auspices of the Heavy Element Chemistry program. Work performed at Los Alamos National Laboratory was under contract with the University of California (Contract No. W-7405-ENG-36). C.N.C. thanks the Seaborg Institute for a postdoctoral fellowship. D.A.S. acknowledges the NSF (CHE-0345263) for support of this work. M.L.K. acknowledges the LANL/UNM Joint Science and Technology Laboratory and the National Science Foundation (NSF CHE-0616190) for support of this work.

Supporting Information Available: Comparison of 30 versus 270 K electronic absorption spectra of Cp*2Yb(tpy) (**7**) as a polystyrene thin film. This information is available free of charge via the Internet at http://pubs.acs.org.

OM061157O

(45) Kirk, M. L.; Shultz, D. A.; Depperman, E. C.; Brannen, C. L. *J. Am. Chem. Soc.* **2007**, *129*, 1937−1943.

(46) Dei, A.; Gatteschi, D.; Sangregorio, C.; Sorace, L.; Vaz, M. G. F. *J. Magn. Magn. Mater.* **2004**, *272/276*, 1083−1084.

(47) Shultz, D. A.; Fico, R. M.; Bodnar, S. H.; Kumar, R. K.; Vostrikova, K. E.; Kampf, J. W.; Boyle, P. D. *J. Am. Chem. Soc.* **2003**, *125*, 11761−11771.

(48) Shultz, D. A.; Fico, R. M.; Lee, H.; Kampf, J. W.; Kirschbaum, K.; Pinkerton, A. A.; Boyle, P. D. *J. Am. Chem. Soc.* **2003**, *125*, 15426−15432.